Published in final edited form as:
J Biomech. 2014 June 27; 47(9): 2013–2021. doi:10.1016/j.jbiomech.2013.10.057.

Functional Analysis of Limb Recovery following Autograft Treatment of Volumetric Muscle Loss in the Quadriceps Femoris

Mon Tzu Alice Li[1,2], **Nick J. Willett**[1,3], **Brent A. Uhrig**[1,3], **Robert E. Guldberg**[1,3], and **Gordon L. Warren**[4,*]

[1]Parker H. Petit Institute for Bioengineering and Bioscience, Georgia Institute of Technology, Atlanta, GA

[2]Wallace H. Coulter Department of Biomedical Engineering, Georgia Institute of Technology & Emory University, Atlanta, GA

[3]George W. Woodruff School of Mechanical Engineering, Georgia Institute of Technology, Atlanta, GA

[4]Department of Physical Therapy, Georgia State University, Atlanta, GA

Abstract

Severe injuries to the extremities often result in muscle trauma and, in some cases, significant volumetric muscle loss (VML). These injuries continue to be challenging to treat, with few available clinical options, a high rate of complications, and often persistent loss of limb function. To facilitate the testing of regenerative strategies for skeletal muscle, we developed a novel quadriceps VML model in the rat, specifically addressing functional recovery of the limb. Our outcome measures included muscle contractility measurements to assess muscle function and gait analysis for evaluation of overall limb function. We also investigated treatment with muscle autografts, whole or minced, to promote regeneration of the defect area. Our defect model resulted in a loss of muscle function, with injured legs generating less than 55% of muscle strength from the contralateral uninjured control legs, even at 4 weeks post-injury. The autograft treatments did not result in significant recovery of muscle function. Measures of static and dynamic gait were significantly decreased in the untreated, empty defect group, indicating a decrease in limb function. Histological sections of the affected muscles showed extensive fibrosis, suggesting that this scarring of the muscle may be in part the cause of the loss of muscle function in this VML model. Taken together, these data are consistent with clinical findings of reduced muscle function in large VML injuries. This new model with quantitative functional outcome measures offers a platform on which to evaluate treatment strategies designed to regenerate muscle tissue volume and restore limb function.

*Author to whom correspondence should be addressed: Department of Physical Therapy, Byrdine F. Lewis School of Nursing and Health Professions, Georgia State University, Atlanta, GA 30302, USA. gwarren@gsu.edu Tel: +1 404 413 1255 .

Conflict of Interest Statement The authors do not have any conflicts of interest to disclose.

Keywords

Volumetric muscle loss; muscle autograft; muscle functional testing; gait analysis; preclinical model

Introduction

Extremity injuries comprise the majority of combat wounds in recent US conflicts, 53% of which are penetrating soft-tissue wounds involving extensive damage to the muscle, also known as volumetric muscle loss (VML) (Owens et al., 2007). Sixty-four percent of all soldiers found unfit for duty are soldiers with extremity injuries, accounting for the majority of the $170 million in projected disability costs (Masini et al., 2009). 12% of civilian patients that had lower extremity trauma experienced VML, and these subsequent treatments resulted in a mean cost of $65,735 (MacKenzie et al., 2000; MacKenzie et al., 2007). Despite the high prevalence and societal cost of VML injuries to the extremities, no tissue engineering treatments are currently available.

Coverage of VML wounds with autogenic muscle flaps is known to be critical in reducing early complications to the healing of soft tissue defects and is the current clinical gold standard (Fischer et al., 1991; Godina et al., 1986). Muscle flap type is a significant predictor of short-term complications (Gopal et al., 2000; Pollak et al., 2000), and muscle coverage aids bone regeneration by increasing bone blood flow (Richards and Schemitsch, 1989; Schemitsch et al., 1997). Other treatment options include the use of sophisticated bracing that allows for physical therapy, but no tissue engineering strategies are available in the clinic thus far (Grogan and Hsu, 2011).

The current treatment options do not take into account structural restoration of muscle, and this is evident in the fact that large muscular defects often lead to persistent functional deficits. High-energy trauma to soft tissues were significantly correlated with poor physical Sickness Impact Profile (SIP) scores—a measure of self-reported physical limitations (MacKenzie et al., 2005). Thirty percent of patients with extensive soft tissue injury reported problems with motility and chronic pain 7-10 years post-injury (Castillo et al., 2006; Giannoudis et al., 2009). An increasing number of VML patients requested late amputations due to functional deficits of the limb (Huh et al., 2011). This persistence of functional deficits highlights the need for functional tissue engineering of VML injuries as well as animal models to quantitatively evaluate regenerative strategies.

Various preclinical VML models have recently been developed to test tissue engineering strategies. Many cell types, such as satellite cells and mesenchymal stem cells, and both natural and synthetic scaffolds have been tested in VML models and shown moderate success in recovering some of the functional deficit caused by the muscle injury (Merritt et al., 2010a; Merritt et al., 2010b; Page et al., 2011; Sicari et al., 2012). The associated studies have used a variety of outcome measures; however, standardized and consistent techniques are not established. As we move forward in refining rat VML models, we seek to increase the relevance to clinical outcomes, in which functional biomechanical testing is critical. Further, many of these models utilize relatively small VML defects in a single muscle – an

injury that may heal without an intervention. In order to further tissue engineering research in VML and to facilitate the translational aspect of these regenerative strategies, there is a need for preclinical models that mimic the complexity and severity of VML injuries observed in the clinic where there is a significant volume of muscle affected including injury to multiple muscles.

Accordingly, our objective was to develop a severe skeletal muscle defect model in the rat incorporating quantitative analysis of muscle regeneration and restoration of limb function. We hypothesized that a full thickness defect through the quadriceps would result in a significant loss of muscle strength and limb function. We further used our model to quantitatively evaluate treatment with muscle autograft, a strategy that has previously been tested in mouse models and shown to improve muscle regeneration (Bierinx and Sebille, 2008). Thus, we hypothesized that an autograft, whether whole or morselized, will significantly increase muscle functional capacity and result in tissue regeneration. We present a very challenging muscle defect rat model that can be used by the scientific community for two important purposes: 1) to further understanding of VML with quantitative measures of the healing process, and 2) to evaluate the success of different muscle regeneration strategies.

Materials and Methods

Surgical Procedure

All surgical procedures were conducted in accordance with guidelines set by the Georgia Tech IACUC (protocol #09039). 13-week-old female Sprague-Dawley rats (Charles River) were randomly assigned to three treatment groups: empty untreated defect (n=12), whole autograft (n=12), and morselized autograft (n=12). For all groups, the muscular injury was performed on the left leg while the right leg served as a non-surgical contralateral control. Muscle defects were created in the quadriceps femoris as previously described (Willett et al., 2013). Briefly, the full-thickness muscular defect comprised of an 8-mm diameter biopsy punch through the medial anterior portion of the quadriceps, affecting parts of all four muscles (Figure 1A, top). In the whole autograft group, the biopsied muscle (Figure 1B, bottom) was placed back into the defect. In the morselized autograft group, biopsied muscle graft was cut into cubes 2 mm in length. All animals were divided into 2 recovery groups: 2-week (n=6 per group) and 4-week (n=6 per group).

Gait Analysis

Gait analysis was performed on all animals pre-surgery (baseline) and at 2 weeks post-injury. Only the 4-week recovery group animals were measured at 4 weeks (Figure 1D). Using the CatWalk 7.1 system (Noldus Information Technology, The Netherlands), quantitative gait measurements were collected. The CatWalk system has previously been validated for assessment of functional limb recovery after sciatic nerve injury (Bozkurt et al., 2008; Deumens et al., 2007; Uhrig et al., 2012) and spinal cord contusion (Hamers et al., 2001). For each data collection, three uninterrupted runs per rat were conducted when possible. Runs that traversed at least half the walkway length were analyzed.

Magnetic Resonance Imaging (MRI)

Three additional animals received empty muscle defects and underwent MR imaging at days 2, 4, 7, and 14 post-injury (Figure 1D); no autograft-treated animals underwent MR imaging. MRI has been shown to be useful in characterizing hematoma or edema formation after muscle injuries (Duda et al., 2008; Lee et al., 2011; Winkler et al., 2011). Images were taken in a 7-tesla MRI system (Pharmascan 7T, Bruker Corp.) and processed in ParaVision 5.1 (BrukerBioSpin, Bruker Corp.). A radiofrequency coil (Doty CP Litzcage coil, 60-mm inner coil diameter) was used for transmitting and receiving signal.T1-weighted images (axial) were taken using a FLASH sequence (TR/TE: 379.5/6.0ms) with 1mm slice thickness. T2-weighted images (axial) were taken using a RARE sequence (TR/TE: 3435.3/52.2ms, rare factor: 6, flip angle: 30 degrees) with 1mm slice thickness. Thirty slices were taken of each leg.

Images were analyzed using ImageJ v1.45 (National Institutes of Health). The volume of interest was determined by using well-defined anatomical structures visible in the T1-weighted images (Figure 2A). VOIs were overlaid on corresponding T2-weighted images (Figure 2B). For uninjured quadriceps femoris muscles, the mean and standard deviation of T2-weighted voxel intensities were used to calculate a threshold value (mean + 2*SD). T2-weighted images of injured muscle were then thresholded (Figure 2B), and voxels with intensities above the threshold indicated hematoma or edema. The volume (V) of hematoma or edema was determined using the trapezoidal interpolation: $V = \left(\sum \left(\frac{A_1 + A_2}{2} \right) * h \right)$, where h is the distance between axial sections and A_1 and A_2 are areas with edema/hematoma of consecutive images.

Measurements of Peak Isometric Contraction Torque about the Knee

At respective recovery time points, 2-week and 4-week rats underwent peak isometric strength measurements, a terminal procedure, to assess the functional capacity of the quadriceps (Figure 1D). An in vivo system similar to those used extensively to assess lower leg muscle function was custom fabricated for assessing torque production about the knee (Lowe et al., 1995; Warren et al., 2004) . Briefly, a nerve cuff was used to stimulate the femoral nerve as a force transducer was used to measure maximal isometric torque production about the knee. Rat movement was restrained (Figure 1B), and the rat ankle was attached to a force transducer (Figure 1C). The nerve was stimulated with progressively increasing voltages to determine the maximum torque.

To assess the fatigability of the quadriceps femoris muscles, the muscle group was subjected to the standard Burke fatigue protocol (Burke et al., 1973). This entailed isometric muscle stimulation with a train consisting of 13 pulses at 25-ms intervals; the train was repeated every second for 2 minutes. The endurance index was calculated as the torque produced at the 1 minute into the protocol divided by the highest torque produced during the protocol. The highest torque was used because varying degrees of potentiation occurred among animals during the first few contractions. Calculation of the endurance index in this manner yielded more reliable values.

Histology

Directly following the measurements of muscle functional capacity, rats were euthanized and underwent perfusion fixation with 10% neutral-buffered formalin (EMD Chemicals, Gibbstown, NJ). The mass of the excised quadriceps was recorded, and the muscle was additionally submersion-fixated in 10% neutral-buffered formalin for 48 hours. Paraffin-processed samples were cut into 5-μm sections using a Microm Microtome (Thermo Scientific, Germany). Hematoxylin and eosin (H&E) staining and Masson's trichrome staining were performed on these sections.

Statistical Analyses

All data are presented as mean ± standard error of the mean. Peak isometric muscle torque and muscle mass were analyzed by a two-way ANOVA (3 treatment groups × 2 time points). Independent t-tests with Bonferroni correction were used to identify within-group differences of recovery time points.

Results

Characterization of early VML with Magnetic Resonance Imaging

Magnetic resonance images were taken at days 2, 4, 7, and 14 post-injury to characterize the muscle injury at early time points. Within the first week of injury, the total muscle volume, quantified by axial T1-weighted images, showed no significant difference between the injured left leg and the contralateral control right leg (Figure 2C). Axial T2-weighted images, in which fluid exhibits increased signal intensity, clearly showed edema/hematoma in the left quadriceps at days 2 and 4 (Figure 2E/F/G/H). This fluid was quantified and comprised the majority of the muscle volume at day 2 post-injury (Figure 2D). This steadily decreased from day 2 to day 14 (Figure 2D).

Measurements of Muscle Functional Capacity

A representative measurement of muscle isometric tetanic torque about the knee is shown in Figure 3A. In all treatment groups, the maximum tetanic torque about the knee from the injured leg was significantly less than the contralateral uninjured leg strength (Figure 3B). A two-way ANOVA on the ratio of injured muscle torque to that of uninjured muscle showed no significant differences between treatment groups or time points; there was no significant recovery of muscle strength in any autograft-treated group from 2 to 4 weeks post-injury (Figure 3C).

Muscle fatigue measurements showed no significant changes in fatigue characteristics between these treatment groups (Supplementary Figure 1). Endurance indices for 2-week fatigue measurements were 0.37 ± 0.08, 0.28 ± 0.13, 0.34 ± 0.08, and 0.26 ± 0.11 for empty, morselized autograft, whole autograft groups, and contralateral controls respectively while 4-week endurance indices were 0.32 ± 0.08, 0.31 ± 0.08, 0.38 ± 0.04, and 0.29 ± 0.08.

Muscle Mass Measurements

Injured muscle from all treatment groups lost a significant amount of muscle mass; the injured muscle had 70-90% of the muscle mass of contralateral controls (Figure 4A). Muscle

mass data of injured muscles normalized to contralateral control muscles showed no significant change in muscle mass between the two time points in any treatment groups (Figure 4B). There was no significant difference in muscle mass between the empty defect group and the treatment groups. Histological cross-sections of muscle tissue at 4 weeks post-injury qualitatively confirmed that injured muscles were similar in size and slightly smaller than a control muscle (Figure 4C). Muscle mass measurements were found to significantly correlate with muscle strength measurements (Supplementary Figure 2) with a correlation coefficient of 0.52.

Measurements of Limb Functionality

Hind paw print area was measured to quantitatively determine limb function in each treatment group. The empty defect group showed a significant decrease in print area ratio (injured to uninjured) compared to baseline control while autograft-treated groups did not show a significant change (Figure 5A). The duty cycle—measurement of the time a paw is contact with the ground as compared to the stride duration—also decreased significantly at 2 and 4 weeks post-injury compared to baseline control (Figure 5B). The whole autograft treated group had a decreased duty cycle at 2 weeks post-injury, compared to the baseline measurements from the same group. Paw print area and duty cycle ratios were found to significantly correlate at weeks 2 and 4, with correlation coefficients of 0.74 and 0.70 respectively (Supplementary Figure 2). 2-week print area and duty cycle ratios and 4-week duty cycle ratios were also found to significantly correlate with the injured leg isometric maximal tetanic torque (Supplementary Figure 2 C, D, F).

Muscle histology

Transverse histological sections were taken from all groups and all time points (Figure 6). Sections stained with H&E showed regenerating muscle fibers with centrally-located nuclei at both time points in all groups. However, sections stained with Masson’s trichrome showed extensive fibrotic tissue formation (indicated by blue staining of collagen) near or surrounding the regenerating muscle fibers. At 4 weeks, the morselized autograft treated group had dispersed fibrotic tissues in small spaces between muscle cells (stained in blue), compared to the large sections of fibrosis seen in the untreated and whole autograft-treated groups.

Discussion

This is, to our knowledge, the first rat model of above-the-knee volumetric skeletal muscle loss. Our model was quantitatively characterized by early analysis of edema and hematoma in the injured muscle using MRI, peak isometric torque produced by the quadriceps femoris, and functional limb analysis as determined by gait. Given the thorough analyses of functional biomechanical outcomes, our model presents a useful platform in which tissue engineering and regenerative medicine strategies can be tested and quantitatively analyzed for efficacy in muscle regeneration.

Our results showed a large decrease in muscle functional capacity, as hypothesized; however, this decrease in muscle function is not wholly explained by the relatively smaller

decrease in muscle mass. One possible explanation is illustrated by Masson's trichrome staining, which showed a large area of blue-stained collagen fibers, indicative of fibrosis of the muscle. Presumably, much of the injured muscle tissue was replaced by fibrotic scar tissue resulting in decreased tissue quality. This non-functional scar tissue in the muscle may account for part of the large functional deficit we see in our model.

Peripheral nerve damage is a likely co-morbidity in our large VML injury. This possible nerve damage further complicates the model and may contribute to the lack of muscle recovery. Denervated muscle flaps have been shown to result in muscle atrophy (Oswald et al., 2004; Yoshitatsu et al., 2008; Zhang et al., 1997). Our model did not exhibit extensive atrophy, suggesting that though peripheral nerve damage may occur, it does not account for the majority of the functional deficit. Nevertheless, reinnervation of motor nerves may enhance muscle regeneration and function (Kaariainen and Kauhanen, 2012) and should be taken into account when developing a treatment strategy for VML.

Clinically, thin muscle flaps that cover large muscle defects are not always effective for functional tissue engineering; thus, we examined the regenerative potential of autografts, which consist of a higher amount of tissue than a muscle flap. Contrary to our hypothesis that this treatment would improve muscle regeneration and function, our VML model showed little to no improvement with autograft treatment. These results seemingly contradict previous literature; the mouse extensor digitorum longus and the rat triceps surae muscles that had been excised, minced, then placed back into its muscle bed regenerated within 2 weeks with little fibrosis (Bierinx and Sebille, 2008) (Carlson and Gutmann, 1972). However, our data showed no significant improvement in muscle function between any treatment groups at any recovery time point. A key difference between the morselized autograft in our model and the minced murine muscle is size. While smaller muscles were able to regenerate with minimal scarring, the larger quadriceps muscle did not reach the same regenerative potential. This is further illustrated in the clinic, where thin muscle flaps are used to cover VML injuries, providing only a small amount of tissue for regeneration with and often resulting in functional deficit.

Another distinct possibility for the lack of functional recovery of the muscle with autograft treatment is related to the muscle extracellular matrix (ECM). In recent years, an increasing number of studies have demonstrated the importance of the ECM in muscle function (Gillies and Lieber, 2011; Meyer and Lieber, 2011). The muscle autografts used in our experiments were not specifically aligned with the muscle fibers within the injury bed, and our VML encompasses parts of all four muscles of the quadriceps, further complicating the orientation of our autograft treatment. This juxtaposition of randomly aligned graft ECM on the muscle ECM may have yielded inefficient functional recovery of the muscle. This lack of recovery with misaligned ECM and the importance of muscle ECM on muscle function suggest that tissue engineering strategies that incorporate structure alignment may result in a more organized tissue and thus a higher chance of functional recovery.

Vascular reconstruction, which is widely used clinically to maintain vascular perfusion in a muscle flap, was not performed in our autograft treatment. The success of muscle flap treatments in the clinic rely heavily on blood supply to the flap. This, again, alludes to the

inversely proportional relationship between VML size and the regenerative potential of the muscle. Research investigating muscle flap treatment of open fractures shows that muscle flaps that are constructed too large suffer from ischemia-induced necrosis (Zahir et al., 1998a, b; Zahir et al., 1998c). Additionally, vascularized muscle flaps that have reconstructed nerve connections served as better wound coverage than disconnected flaps, suggesting that vascularization and nerves play a role in survival of the graft (Kaariainen and Kauhanen, 2012). The autografts used in our model may have necrosed from lack of intact vessels, leading to an inflammatory environment that may have deterred any healing response from stem cells or extracellular matrix proteins in the autograft. This suggests that regenerative approaches that facilitate vascular growth may increase the survival rate of implanted or migrated endogenous cells in the center of the VML defect.

As mentioned before, our minced and whole autograft treatments of the VML defect illustrated the importance of differences in mass and nutrient transfer that arise from the size scale of the muscle defect and the animal model . While minced and whole autografts did not result in functional regeneration in our rat quadriceps defect model, another group has demonstrated some success of this therapy in the tibialis anterior muscle of the rat, in which a smaller, single-muscle VML was created (Corona et al., 2013). Additionally, while ECM treatment has had moderate success in regenerating muscles in rodent models, the same treatment used in the dog gastrocnemius muscle resulted in little recovery in the muscle function after 3 months (Turner et al., 2012; Turner et al., 2010). This, again, highlights the need for a large, challenging regenerative environment in preclinical models to maximize translational potential of therapies.

Various tissue engineering strategies have been tested in preclinical models of VML that have shown promising effects on muscle regeneration. Small intestinal submucosa extracellular matrices (SIS-ECM) have been tested in a mouse quadriceps VML, and host skeletal muscle cells infiltrated the ECM, indicating possible muscle regeneration though no muscle function was tested (Sicari et al., 2012). Other groups have decellularized the rat gastrocnemius muscle and then recellularized this ECM with mesenchymal stem cells (MSCs). When implanted in a rat gastrocnemius defect, this treatment showed significant functional recovery compared to ECM or injury alone (Merritt et al., 2010a; Merritt et al., 2010b). Other promising interventions have used muscle-derived stem cells or satellite cells seeded on fibrin microthreads or hyaluoronic acid hydrogel respectively; both studies showed functional recovery when implanted in a mouse tibialis anterior muscle VML model (Page et al., 2011; Rossi et al., 2011). These regenerative strategies clearly have potential for the functional healing; however, the VML used to test these treatments were relatively small. Given the size considerations of VML models, it would be beneficial to test strategies such as these in our challenging VML in order to rigorously filter preclinical treatments prior to investigating their potential in even larger animal models or humans.

Conclusion

We have successfully established a novel model of VML in the quadriceps femoris of a rat with quantitative functional outcome metrics. Contrary to our hypothesis, neither minced nor whole autografts resulted in any significant recovery of muscle function. This is consistent

with clinical outcomes, in which autogenic muscle flap treatments of VML injuries often result in functional deficits. The large deficit shown by our model demonstrates the lack of functional recovery, emphasizing the need for translational regenerative strategies for VML.

Supplementary Material

Refer to Web version on PubMed Central for supplementary material.

Acknowledgments

This work was supported by the U.S. Army Medical Research and Materiel Command (W81XWH-10-2-0006), the National Institute of Health (Grant #1F32AR061236-01), and the NIH Cell and Tissue Engineering training grant (NIH T32 GM008433).

REFERENCES

Bierinx AS, Sebille A. Mouse sectioned muscle regenerates following auto-grafting with muscle fragments: a new muscle precursor cells transfer? Neuroscience letters. 2008; 431:211–214. [PubMed: 18178008]

Bozkurt A, Deumens R, Scheffel J, O'Dey DM, Weis J, Joosten EA, Fuhrmann T, Brook GA, Pallua N. CatWalk gait analysis in assessment of functional recovery after sciatic nerve injury. J Neurosci Methods. 2008; 173:91–98. [PubMed: 18577402]

Burke RE, Levine DN, Tsairis P, Zajac FE 3rd. Physiological types and histochemical profiles in motor units of the cat gastrocnemius. J Physiol. 1973; 234:723–748. [PubMed: 4148752]

Carlson BM, Gutmann E. Development of contractile properties of minced muscle regenerates in the rat. Experimental neurology. 1972; 36:239–249. [PubMed: 5053353]

Castillo RC, MacKenzie EJ, Wegener ST, Bosse MJ. Prevalence of chronic pain seven years following limb threatening lower extremity trauma. Pain. 2006; 124:321–329. [PubMed: 16781066]

Corona BT, Garg K, Ward CL, McDaniel JS, Walters TJ, Rathbone CR. Autologous minced muscle grafts: A tissue engineering therapy for the volumetric loss of skeletal muscle. American journal of physiology. Cell physiology. 2013

Deumens R, Jaken RJ, Marcus MA, Joosten EA. The CatWalk gait analysis in assessment of both dynamic and static gait changes after adult rat sciatic nerve resection. J Neurosci Methods. 2007; 164:120–130. [PubMed: 17532474]

Duda GN, Taylor WR, Winkler T, Matziolis G, Heller MO, Haas NP, Perka C, Schaser KD. Biomechanical, microvascular, and cellular factors promote muscle and bone regeneration. Exercise and sport sciences reviews. 2008; 36:64–70. [PubMed: 18362687]

Fischer MD, Gustilo RB, Varecka TF. The timing of flap coverage, bone-grafting, and intramedullary nailing in patients who have a fracture of the tibial shaft with extensive soft-tissue injury. J Bone Joint Surg Am. 1991; 73:1316–1322. [PubMed: 1918113]

Giannoudis PV, Harwood PJ, Kontakis G, Allami M, Macdonald D, Kay SP, Kind P. Long-term quality of life in trauma patients following the full spectrum of tibial injury (fasciotomy, closed fracture, grade IIIB/IIIC open fracture and amputation). Injury. 2009; 40:213–219. [PubMed: 19070847]

Gillies AR, Lieber RL. Structure and function of the skeletal muscle extracellular matrix. Muscle Nerve. 2011; 44:318–331. [PubMed: 21949456]

Godina M, Bajec J, Baraga A. Salvage of the mutilated upper extremity with temporary ectopic implantation of the undamaged part. Plast Reconstr Surg. 1986; 78:295–299. [PubMed: 3737753]

Gopal S, Majumder S, Batchelor AG, Knight SL, De Boer P, Smith RM. Fix and flap: the radical orthopaedic and plastic treatment of severe open fractures of the tibia. J Bone Joint Surg Br. 2000; 82:959–966. [PubMed: 11041582]

Grogan BF, Hsu JR. Volumetric muscle loss. J Am Acad Orthop Surg. 2011; 19(Suppl 1):S35–37. [PubMed: 21304045]

Hamers FP, Lankhorst AJ, van Laar TJ, Veldhuis WB, Gispen WH. Automated quantitative gait analysis during overground locomotion in the rat: its application to spinal cord contusion and transection injuries. J Neurotrauma. 2001; 18:187–201. [PubMed: 11229711]

Huh J, Stinner DJ, Burns TC, Hsu JR. Infectious complications and soft tissue injury contribute to late amputation after severe lower extremity trauma. J Trauma. 2011; 71:S47–51. [PubMed: 21795878]

Kaariainen M, Kauhanen S. Skeletal muscle injury and repair: the effect of disuse and denervation on muscle and clinical relevance in pedicled and free muscle flaps. Journal of reconstructive microsurgery. 2012; 28:581–587. [PubMed: 22711205]

Lee YS, Kwon ST, Kim JO, Choi ES. Serial MR imaging of intramuscular hematoma: experimental study in a rat model with the pathologic correlation. Korean journal of radiology : official journal of the Korean Radiological Society. 2011; 12:66–77. [PubMed: 21228942]

Lowe DA, Warren GL, Ingalls CP, Boorstein DB, Armstrong RB. Muscle function and protein metabolism after initiation of eccentric contraction-induced injury. Journal of applied physiology. 1995; 79:1260–1270. [PubMed: 8567571]

MacKenzie EJ, Bosse MJ, Kellam JF, Burgess AR, Webb LX, Swiontkowski MF, Sanders RW, Jones AL, McAndrew MP, Patterson TM, McCarthy ML. Characterization of patients with high-energy lower extremity trauma. J Orthop Trauma. 2000; 14:455–466. [PubMed: 11083607]

MacKenzie EJ, Bosse MJ, Pollak AN, Webb LX, Swiontkowski MF, Kellam JF, Smith DG, Sanders RW, Jones AL, Starr AJ, McAndrew MP, Patterson BM, Burgess AR, Castillo RC. Long-term persistence of disability following severe lower-limb trauma. Results of a seven-year follow-up. J Bone Joint Surg Am. 2005; 87:1801–1809. [PubMed: 16085622]

MacKenzie EJ, Jones AS, Bosse MJ, Castillo RC, Pollak AN, Webb LX, Swiontkowski MF, Kellam JF, Smith DG, Sanders RW, Jones AL, Starr AJ, McAndrew MP, Patterson BM, Burgess AR. Health-care costs associated with amputation or reconstruction of a limb-threatening injury. J Bone Joint Surg Am. 2007; 89:1685–1692. [PubMed: 17671005]

Masini BD, Waterman SM, Wenke JC, Owens BD, Hsu JR, Ficke JR. Resource utilization and disability outcome assessment of combat casualties from Operation Iraqi Freedom and Operation Enduring Freedom. J Orthop Trauma. 2009; 23:261–266. [PubMed: 19318869]

Merritt EK, Cannon MV, Hammers DW, Le LN, Gokhale R, Sarathy A, Song TJ, Tierney MT, Suggs LJ, Walters TJ, Farrar RP. Repair of traumatic skeletal muscle injury with bone-marrow-derived mesenchymal stem cells seeded on extracellular matrix. Tissue engineering. Part A. 2010a; 16:2871–2881. [PubMed: 20412030]

Merritt EK, Hammers DW, Tierney M, Suggs LJ, Walters TJ, Farrar RP. Functional assessment of skeletal muscle regeneration utilizing homologous extracellular matrix as scaffolding. Tissue engineering. Part A. 2010b; 16:1395–1405. [PubMed: 19929169]

Meyer GA, Lieber RL. Elucidation of extracellular matrix mechanics from muscle fibers and fiber bundles. J Biomech. 2011; 44:771–773. [PubMed: 21092966]

Oswald TM, Zhang F, Lei MP, Gerzenshtein J, Lineaweaver WC. Muscle flap mass preservation with end-to-side neurorrhaphy: an experimental study. Journal of reconstructive microsurgery. 2004; 20:483–488. [PubMed: 15356771]

Owens BD, Kragh JF Jr. Macaitis J, Svoboda SJ, Wenke JC. Characterization of extremity wounds in Operation Iraqi Freedom and Operation Enduring Freedom. J Orthop Trauma. 2007; 21:254–257. [PubMed: 17414553]

Page RL, Malcuit C, Vilner L, Vojtic I, Shaw S, Hedblom E, Hu J, Pins GD, Rolle MW, Dominko T. Restoration of skeletal muscle defects with adult human cells delivered on fibrin microthreads. Tissue engineering. Part A. 2011; 17:2629–2640. [PubMed: 21699414]

Pollak AN, McCarthy ML, Burgess AR. Short-term wound complications after application of flaps for coverage of traumatic soft-tissue defects about the tibia. The Lower Extremity Assessment Project (LEAP) Study Group. J Bone Joint Surg Am. 2000; 82-A:1681–1691. [PubMed: 11130641]

Richards RR, Schemitsch EH. Effect of muscle flap coverage on bone blood flow following devascularization of a segment of tibia: an experimental investigation in the dog. J Orthop Res. 1989; 7:550–558. [PubMed: 2738772]

Rossi CA, Flaibani M, Blaauw B, Pozzobon M, Figallo E, Reggiani C, Vitiello L, Elvassore N, De Coppi P. In vivo tissue engineering of functional skeletal muscle by freshly isolated satellite cells embedded in a photopolymerizable hydrogel. FASEB journal : official publication of the Federation of American Societies for Experimental Biology. 2011; 25:2296–2304. [PubMed: 21450908]

Schemitsch EH, Weinberg JA, McKee MD, Richards RR. The relative importance of intramedullary, intracortical, and extraosseous soft-tissue blood flow to the repair of devascularized canine tibial cortex. Ann Plast Surg. 1997; 38:623–631. [PubMed: 9188979]

Sicari BM, Agrawal V, Siu BF, Medberry CJ, Dearth CL, Turner NJ, Badylak SF. A murine model of volumetric muscle loss and a regenerative medicine approach for tissue replacement. Tissue engineering. Part A. 2012; 18:1941–1948. [PubMed: 22906411]

Turner NJ, Badylak JS, Weber DJ, Badylak SF. Biologic scaffold remodeling in a dog model of complex musculoskeletal injury. The Journal of surgical research. 2012; 176:490–502. [PubMed: 22341350]

Turner NJ, Yates AJ Jr. Weber DJ, Qureshi IR, Stolz DB, Gilbert TW, Badylak SF. Xenogeneic extracellular matrix as an inductive scaffold for regeneration of a functioning musculotendinous junction. Tissue engineering. Part A. 2010; 16:3309–3317. [PubMed: 20528669]

Uhrig BA, Clements IP, Boerckel JD, Huebsch N, Bellamkonda RV, Guldberg RE. Characterization of a composite injury model of severe lower limb bone and nerve trauma. Journal of tissue engineering and regenerative medicine. 2012

Warren GL, Stallone JL, Allen MR, Bloomfield SA. Functional recovery of the plantarflexor muscle group after hindlimb unloading in the rat. Eur J Appl Physiol. 2004; 93:130–138. [PubMed: 15248071]

Willett NJ, Li MT, Uhrig BA, Boerckel JD, Huebsch N, Lundgren TL, Warren GL, Guldberg RE. Attenuated human bone morphogenetic protein-2-mediated bone regeneration in a rat model of composite bone and muscle injury. Tissue engineering. Part C, Methods. 2013; 19:316–325. [PubMed: 22992043]

Winkler T, von Roth P, Matziolis G, Schumann MR, Hahn S, Strube P, Stoltenburg-Didinger G, Perka C, Duda GN, Tohtz SV. Time course of skeletal muscle regeneration after severe trauma. Acta Orthop. 2011; 82:102–111. [PubMed: 21142822]

Yoshitatsu S, Matsuda K, Yano K, Hosokawa K, Tomita K. Muscle flap mass preservation by sensory reinnervation with end-to-side neurorrhaphy: an experimental study in rats. Journal of reconstructive microsurgery. 2008; 24:479–487. [PubMed: 18798137]

Zahir KS, Syed SA, Zink JR, Restifo RJ, Thomson JG. Comparison of the effects of ischemic preconditioning and surgical delay on pedicled musculocutaneous flap survival in a rat model. Ann Plast Surg. 1998a; 40:422–428. discussion 428-429. [PubMed: 9555999]

Zahir KS, Syed SA, Zink JR, Restifo RJ, Thomson JG. Ischemic preconditioning improves the survival of skin and myocutaneous flaps in a rat model. Plast Reconstr Surg. 1998b; 102:140–150. discussion 151-142. [PubMed: 9655419]

Zahir TM, Zahir KS, Syed SA, Restifo RJ, Thomson JG. Ischemic preconditioning of musculocutaneous flaps: effects of ischemia cycle length and number of cycles. Ann Plast Surg. 1998c; 40:430–435. [PubMed: 9556000]

Zhang F, Lineaweaver WC, Ustuner T, Kao SD, Tonken HP, Campagna-Pinto D, Buncke HJ. Comparison of muscle mass preservation in denervated muscle and transplanted muscle flaps after motor and sensory reinnervation and neurotization. Plast Reconstr Surg. 1997; 99:803–814. [PubMed: 9047201]

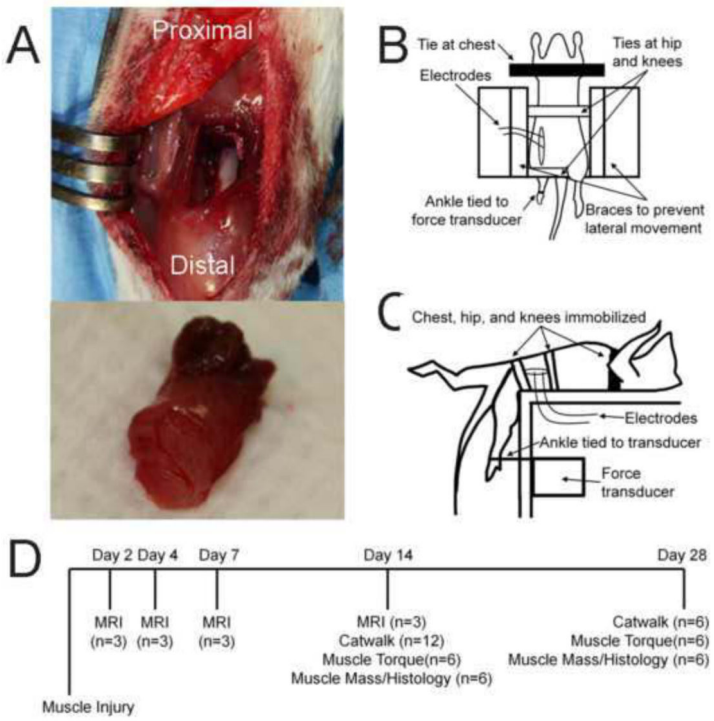

Figure 1. Methods

A. Representative images showing the muscle defect surgery (top) and excised 8-mm diameter muscle (bottom). **B.** Representative diagram of the top-down view of muscle strength measurements. **C.** Representative diagram of the side view of muscle strength measurements. **D.** Timeline of longitudinal in vivo (MRI, Catwalk) and ex vivo (muscle torque, muscle mass, histology) measurements, with samples sizes, for the whole study.

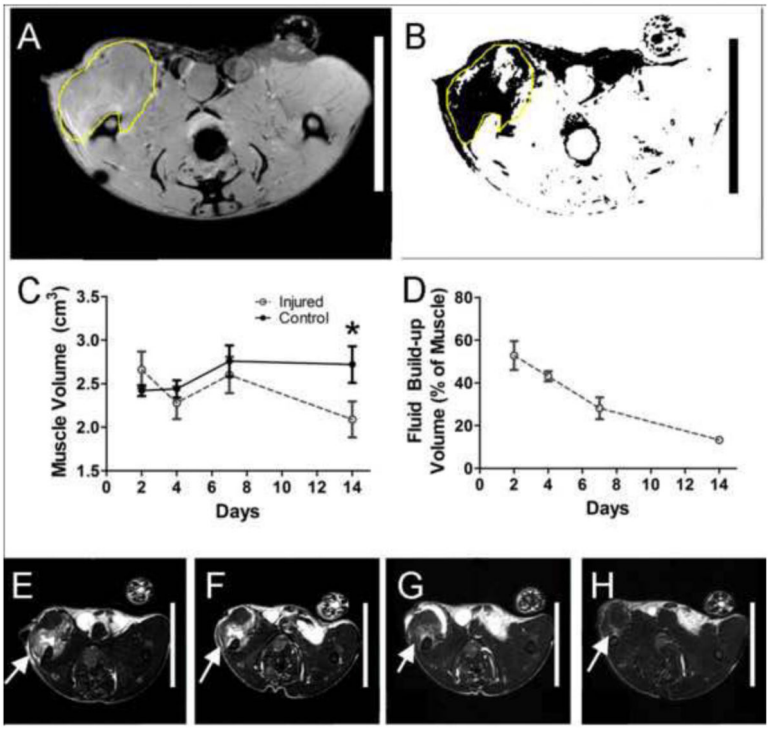

Figure 2. MRI Visualization of the Extent of Muscle Injury

A. Representative selection of region of interest using T1-weighted image. **B.** Representative superposition of ROI on thresholded T2-weighted image. Dark pixels indicate pixels with intensities above threshold. **C.** Total muscle volume, measured using axial T_1-weighted MRI images. **D**. Percentage of the left leg muscle that was inflamed, as determined by edema in the quadriceps area visualized by T_2-weighted images. **E-H.** Representative T_2-weighted images at days 2 (E), 4 (F), 7 (G), and 14 (H) days are shown, with inflamed areas indicated by white arrows. *$p<0.05$, n=3, ANOVA with Bonferroni correction.

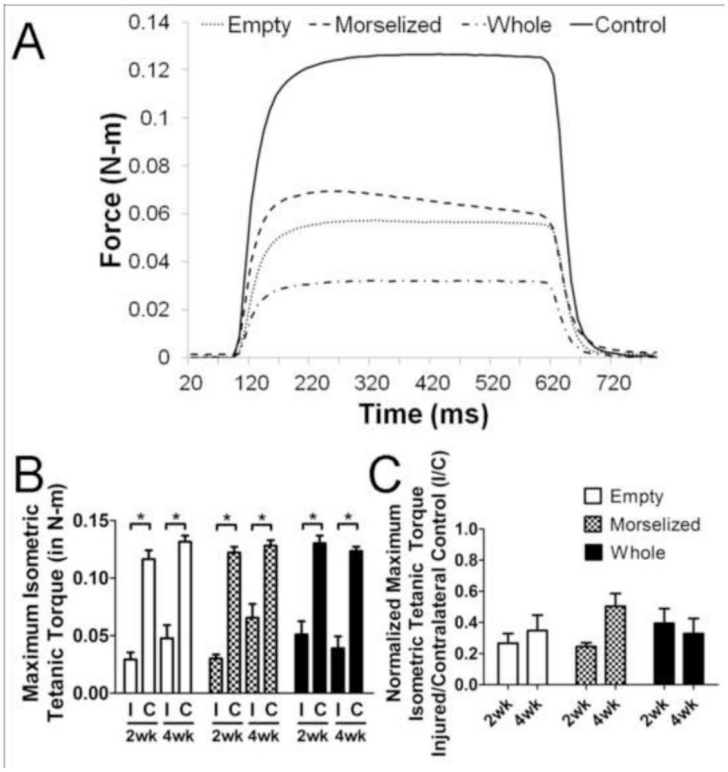

Figure 3. Quantitative Measures of Muscle Function

A. Representative graph of tetanic muscle torque measurement for empty defect (dotted), morselized autograft (dash), whole autograft (dash-dot-dash), and unoperated control (solid) groups. **B.** Maximum isometric tetanic torque of the quadriceps muscle in the injured left leg (I) and contralateral control right leg (C). **C.** Muscle torque expressed as a ratio of the injured leg to contralateral control (I/C). *$p<0.05$, n=6 per group per time point.

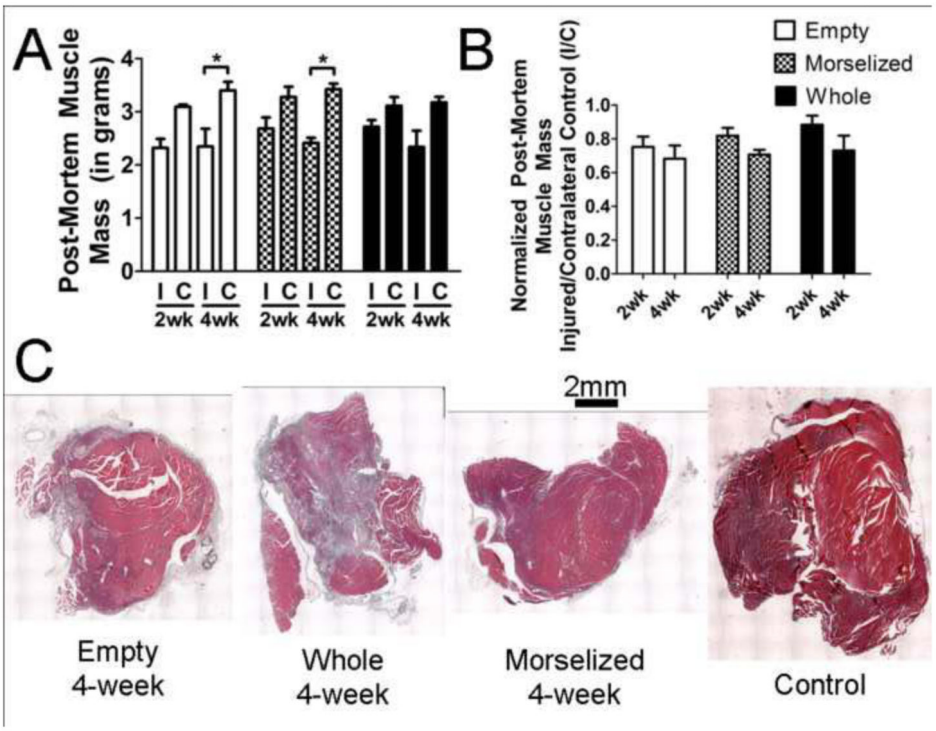

Figure 4. Muscle Mass and Representative Cross-Sectional Images of Muscle

A. Post-mortem muscle mass of the quadriceps muscle from the injured left leg (I) and contralateral control right leg (C). **B.** Post-mortem muscle mass expressed as a ratio of the injured leg to contralateral control (I/C). **C.** Representative H&E stained transverse (cross-sections) images of muscles from all treatment groups and control. *$p<0.05$, n=6 per group per time point.

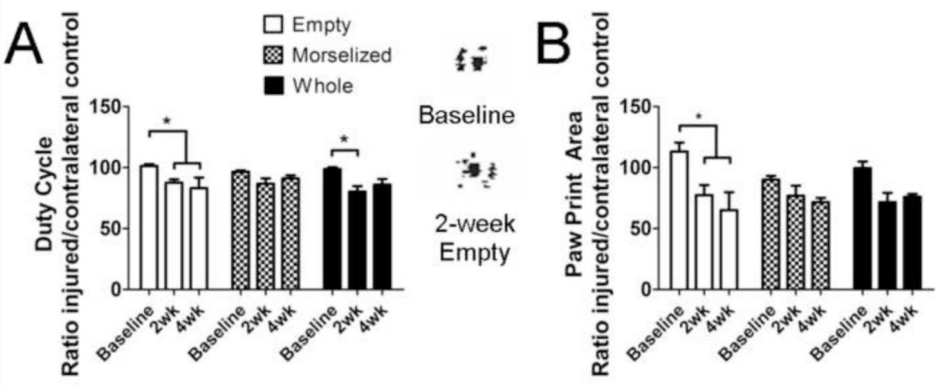

Figure 5. Quantitative Measures of Gait and Limb Recovery

A. Print area, a static gait parameter, at baseline (measured prior to surgery), 2 weeks, and 4 weeks post injury. Representative paw prints are shown on the right. **B.** Duty cycle, a dynamic gait parameter that measures the time a paw is in contact with the ground as compared to stride duration. *$p<0.05$, n=12 at 2 weeks, n=6 at 4 weeks

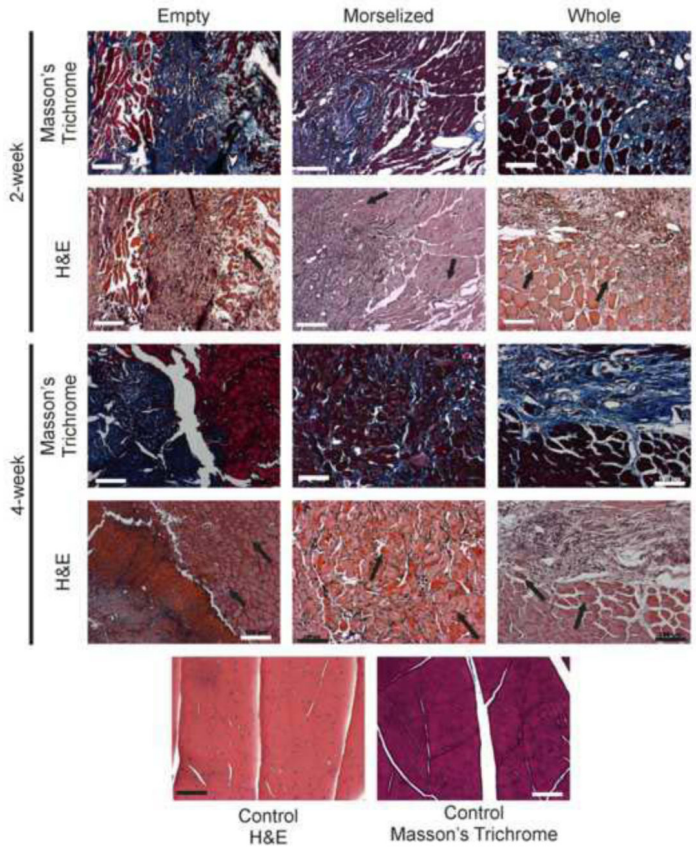

Figure 6. Fibrosis and regenerating fibers, visualized in histology

Fibrosis can be seen in Masson's Trichrome stained sections (collagen fibers stain blue). Regenerating muscle fibers, in which nuclei are centrally located, can be seen in H&E stained sections (indicated by black arrows). Images were taken at 10x magnification, scale bars: 100μm.